

Temperature Dependent Current Dispersion Study in β -Ga₂O₃ FETs Using Sub-Microsecond Pulsed IV Characteristics

Abhishek Vaidya, and Uttam Singiseti

Abstract—A comprehensive study of drain current dispersion effects in β -Ga₂O₃ FETs has been done using DC, pulsed and RF measurements. Both virtual gate effect in the gate-drain access region and interface traps under the gate are most plausible explanations for the experimentally observed pulsed current dispersion and high temperature threshold voltage shift respectively. Unpassivated devices show significant current dispersion between DC and pulsed IV response due to gate lag effect characterized by time constants in the range of 400 μ s to 600 μ s. An activation energy of 99 meV is estimated from temperature dependent Arrhenius plots. A variable range hopping based slow transport in conjunction with the observed shallow trap level is attributed to the observed slow transient response of drain current with respect to time. Reactive ion etching step during the device fabrication is most likely responsible for introducing the traps. Effect of traps can be minimized by using surface passivation layers, in this case, Silicon Nitride which shows significant improvement in the current dispersion and RF cutoff frequency. This work demonstrates the detrimental effect the traps can have on the current dispersion which significantly limits the high frequency operation of the device.

Index Terms— β -Ga₂O₃, current dispersion, Interface traps, Pulsed IV, Virtual gate

I. INTRODUCTION

BETA Gallium oxide has garnered a lot of interest of researchers across the globe because of its attractive material properties such as ultra-wide bandgap of ~ 4.8 - 4.9 eV [1], [2], good electron mobility, high breakdown field strength of 8 MV/cm [3]–[6], and also the ease of growing high quality epitaxial films with controllable doping [7]–[14] on melt grown bulk crystals. The large breakdown field strength translates to high Baliga's Figure of Merit (*BFoM*) making it superior candidate for power device applications. Several groups have demonstrated kilovolt class field effect transistors (FETs) and Schottky diodes [15]–[27]. In addition, β -Ga₂O₃ also has a high Johnson's Figure of Merit (*JFoM*) owing to

the large calculated electron velocity [28], which has been experimentally verified [29]. High *JFoM* implies β -Ga₂O₃ is also suitable for high frequency devices such as GHz switches and RF amplifiers. Recently a few groups have successfully demonstrated β -Ga₂O₃ field effect transistors with current gain cutoff frequencies (f_t) in the GHz range [30]–[32]. Xia *et.al.* reported the highest f_t of 27 GHz in a delta doped β -Ga₂O₃ (Ga₂O₃)FET with regrown ohmic contacts [33].

In addition to the cutoff frequencies, another important factor for high frequency performance of the device is DC to RF drain current dispersion which causes transconductance to collapse as the frequency of operation increases with an associated knee-walk off phenomenon. This is primarily caused by interface and/or bulk traps which act as generation and recombination centers. The time constant associated with the traps dictates the amount of dispersion at an given frequency. Transient response analysis using pulsed current-voltage measurements is a popular method to identify the type and location, both physical and energy, of the trap. This method has been widely used to study dispersion in GaN based devices [34]–[39]. While, only a few reports exist on Ga₂O₃ devices.

There are two kinds of β -Ga₂O₃ RF FET devices reported; namely, (a) the source/drain (S/D) regions are either regrown or ion implanted and (b) the S/D n⁺ layers grown and then removed from the channel region by reactive ion etching (RIE) which are called recessed gate FETs. The recessed gate process requires channel to be exposed to reactive ion etching which has been identified to introduce plasma damage and interface states [40]–[43]. This makes it vital to study the effect of traps and find ways to mitigate their detrimental effects on the device performance. There have been very few studies specifically on β -Ga₂O₃ devices. Moser *et. al.* [44] have reported pulsed large signal power performance of β -Ga₂O₃ MOSFET. They have analyzed continuous and pulsed output power to provide evidence of presence of traps for the observed dispersion. In contrast, in a previous report, Moser *et. al.* show pulsed current voltage characterization on a 200 nm bulk channel FET which shows no appreciable current dispersion [45]. A pulsed large signal RF performance was reported by Singh *et. al.* [46] which shows negligible DC-RF dispersion with microsecond pulses. McGlone *et. al.* explore buffer traps in a δ doped β -Ga₂O₃ structure using Deep Level Transient spectroscopy and double pulsed I-V measurements [47]–[49]. Joishi *et. al.* report double pulsed

We acknowledge the support from Air Force Office of Scientific Research under award number FA9550-18-1-0479 (Program Manager: Ali Sayir) and from NSF under awards ECCS 1607833 and ECCS - 1809077. This work was performed partly at Shared Instrumentation Lab, University at Buffalo. This research used resources of the Center for Functional Nanomaterials, which is a U.S. DOE Office of Science Facility, at Brookhaven National Laboratory under Contract No. DE-SC0012704 & Center for Functional Nanomaterial, Brookhaven National Lab.

Abhishek Vaidya & Uttam Singiseti are with Electrical Engineering Department, University at Buffalo, Buffalo, NY - 14260

current voltage measurement using a $5 \mu s$ pulse width on a Si δ -doped β - Ga_2O_3 FET which shows drastic improvement in current after *in-situ* passivation [50]. Nevertheless, significant knowledge gap exists in the DC-RF dispersion and mitigation strategies for Ga_2O_3 FET devices. In this work, we report a comprehensive temperature dependent DC-RF dispersion analysis in Ga_2O_3 MOSFETs using a minimum pulse width of $200 ns$. We provide the origin of the DC-RF dispersion and the nature and location of traps along with the mechanism of capture and emission processes. We also first report the effectiveness of silicon nitride passivation in reducing the DC-RF current dispersion in Ga_2O_3 MOSFETs.

II. EXPERIMENTAL DETAILS

The semi-insulating Ga_2O_3 substrates used in this study were grown by edge defined film fed growth method by Tamura Corporation, Japan. Device quality channel and ohmic capping epilayers were grown homoepitaxially on top of $200 nm$ unintentionally doped (UID) Ga_2O_3 to act as a buffer layer. All the device layers including UID were grown by ozone molecular beam epitaxy (MBE). A gas mixture of ozone and oxygen was used as the oxygen source. The substrate temperature was $700^\circ C$, and the growth rate of Ga_2O_3 was $0.6 \mu m/hr$. The channel and ohmic capping layer were grown with target thickness and doping concentrations of $200 nm / 7 \times 10^{17} cm^{-3}$ and $50 nm / 1 \times 10^{19} cm^{-3}$ respectively. Fig.1 shows the schematic of the device fabrication, electron beam lithography (EBL) was used in all the steps. Device isolation etch was first performed using inductively coupled plasma reactive ion etching (ICP RIE) with BCl_3/Ar chemistry. Next, $Ti/Au/Ni$ source and drain contacts were deposited by e-beam evaporation followed by a $1 min / 520^\circ C$ N_2 anneal to aid the formation of ohmic contacts. Followed by this, BCl_3/Ar gate recess etch was performed between source and drain ($L_{sd} = 0.5 \mu m$) to remove the highly doped ohmic capping layer. A $20 nm$ plasma ALD SiO_2 was deposited as a gate dielectric layer and subsequently annealed at $450^\circ C$ to improve its dielectric properties. Another lithography was performed to remove the oxide from source and drain contact pads, this time, using CF_4/Ar chemistry in ICP RIE. Finally a Ti/Au gate contact pad and gate were deposited to complete the fabrication for the pre-passivation study. SEM micrographs were imaged using Carl Zeiss AURIGA CrossBeam. A $250 nm$ thick plasma enhanced chemical vapor deposition (PECVD) silicon nitride (SiN_x) was deposited to study the passivation of the interface states. The SiN_x was removed from the source/drain and gate contact pads to facilitate the probing.

For DC current-voltage (I-V) measurements HP4155B semiconductor parameter analyzer was used. A MS-TECH 1000H temperature controlled stage was used to measure up to $300^\circ C$. Pulsed IV measurements were done using an Auriga AU-5 high voltage pulsed IV setup capable of sourcing $100 V/200 ns$ at input port and $200 V/200 ns$ at output port with $20 ns$ rise and fall time. The device was probed using a co-planar waveguide (CPW) RF probes to ensure minimum reflections at the probe-device interface (See Fig. 2).

To analyze the trapping/detrapping response of traps, the

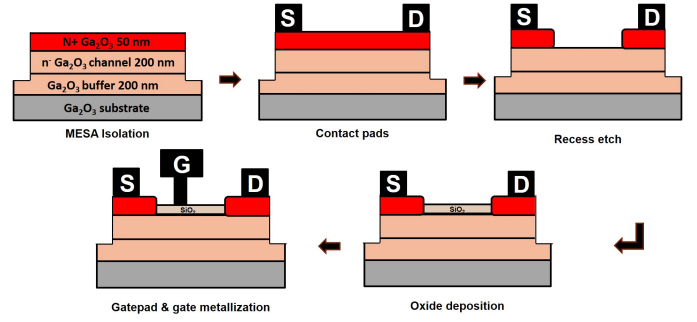


Fig. 1. The figure highlights major steps in fabrication process flow of the device in this study.

well known gate-lag and drain-lag measurement technique was implemented as follows:

- **Gate turn-on:** Gate bias is pulsed from off state ($V_g = -25 V$) to on state ($V_g = 0 V$) while maintaining a constant drain bias. Complete IV curves are obtained by sweeping V_d from $0 V$ to $7 V$.
- **Drain turn-on:** Drain bias is pulsed from off state ($V_d = 0 V$) to on state ($V_d = 7 V$) while maintaining a constant gate bias. Complete IV curves are obtained by sweeping V_g from $-25 V$ to $0 V$.

For each study, pulse width was varied from $200 ns$ to $1 ms$ with a pulse period of $20 ms$ to allow sufficient time for the traps to regain their original state after every on pulse. The low duty cycle also ensures device self-heating effects are minimized. The number of samples were varied between 40 and 2000 based on the pulse width with highest samples for $1 ms$ pulse and lowest samples for $200 ns$ pulse. For each pulsed measurement, the recorded I_d value was averaged over last 10% time window of the pulse. The measurements were repeated for high temperatures up to $200^\circ C$ before and after passivation.

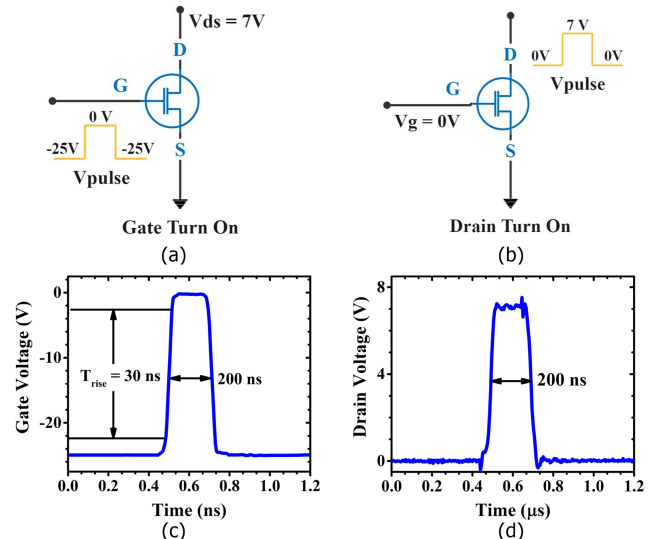


Fig. 2. (a) & (b) show schematic representation of measurement setups for gate and drain turn on measurements respectively. (c) & (d) show $200 ns$ gate and drain input voltage pulse shapes.

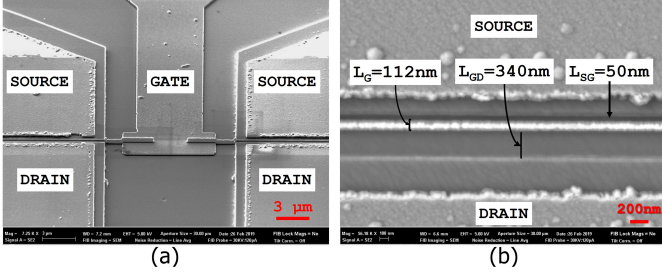


Fig. 3. (a) SEM micrograph of the device showing large source and drain contact pads. (b) Zoomed in SEM view of the gate recess region showing intrinsic part of the device.

S-parameter measurements were carried out using *Agilent E5071* series ENA. The measurements were repeated after passivation.

III. RESULTS AND DISCUSSIONS

The final dimensions of the fabricated device are; gate length (L_g) = 112 nm, Source-Gate spacing (L_{sg}) = 50 nm and Gate-Drain spacing (L_{gd}) = 340 nm. Fig.3 shows SEM micrograph of the fabricated device.

A. DC I-V Analysis

Fig. 4(a) and (b) show the measured I_d - V_d characteristics at room temperature and 200°C respectively. At room temperature we see incomplete turnoff even at $V_g = -25V$. It is attributed to the moderately high doping in the channel, a thicker channel and a smaller gate length resulting in a reduced control over the channel current. Gate voltages lower than -25 V were avoided to protect devices from gate dielectric electrical breakdown. The short channel effects are also evident due to shorter gate length. A maximum current of 210 mA/mm was recorded for this device at $V_g = 0V$. Non-ideal behaviour of source-drain contacts can also be seen in the graph which is a consequence of non-optimized contact formation process. This also results in higher source and drain resistances which reduces the net drain current and transconductance. The device shows improved ON/OFF ratio at 200°C for the same V_g as indicated in Fig. 4(b) (solid red line) which is due to a threshold voltage shift that can be attributed to mobile trapped charges in the gate oxide. Contact linearity is improved at this temperature most likely due to reduced thermionic emission

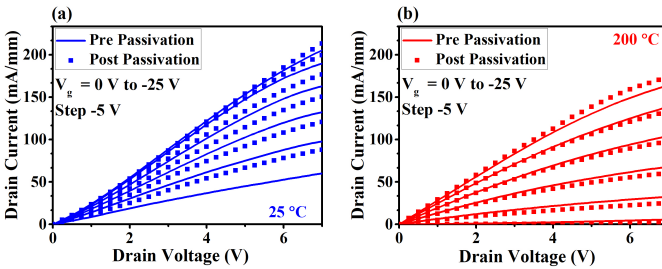


Fig. 4. (a) Static I_d - V_d comparison before the passivation (line) and after passivation (symbol) at room temperature. (b) Static I_d - V_d comparison before the passivation (line) and after passivation (symbol) at 200°C.

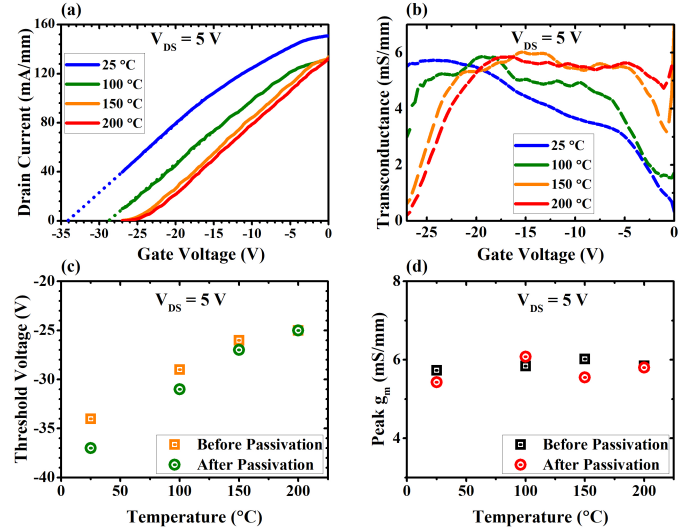


Fig. 5. (a) I_d - V_g (left) and corresponding (b) g_m - V_g (right) plots before passivation at room temperature (blue), 100°C (green), 150°C (orange), and 200°C (red). (c) V_t shift with temperature data before and after passivation shows a similar monotonic positive shift in V_t (d) Peak g_m vs Temperature data before and after passivation indicates little to no change in maximum static g_m .

barrier. The figures also show that there is a small change in DC I-V characteristics after SiN_x passivation.

Fig. 5(a) and (b) show temperature dependent I_d - V_g and g_m - V_g plots respectively, at $V_{ds} = 5V$, before passivation. The positive shift in the threshold voltage is evident again suggesting presence of trapped charges in the gate oxide. A maximum g_m of 6 mS/mm has been recorded which as discussed earlier is a considerably lower value for designed device dimensions due to higher source and drain access resistances. As seen in the temperature dependent threshold and peak g_m plots in Fig. 5 (c) & (d), the passivation does not reduce the threshold voltage shift with temperature. This is again due to the fact the traps under the gate are unaffected by passivation. The peak value of g_m also remains largely unaffected after passivation.

B. Pulsed I-V Analysis

As described in the Introduction, pulsed I-V analysis is important to study the DC to RF dispersion that arise from the dynamic response of traps with change in bias. We carried out drain turn on and gate turn on pulsing individually to isolate the effects of interface traps and bulk traps and localize the source of current dispersion.

Drain Turn On: We first discuss the drain pulse measurements, as the bulk traps are expected to respond to drain pulse [51], [52]. Fig. 6 (a) shows device response to drain turn on pulse before passivation showing negligible dispersion in the I_d - V_d plots for different pulse widths. Fig. 6 (b) shows the drain current pulse which does not show any delays in either transient edges. This rules out presence of any significant buffer traps. Fe diffusion from substrate has been identified as a trap in MBE grown Ga_2O_3 devices [47]. However, the ozone MBE growth of the Ga_2O_3 does not show any appreciable Fe diffusion as seen in Fig. 3 in Ref. [53]. The same growth

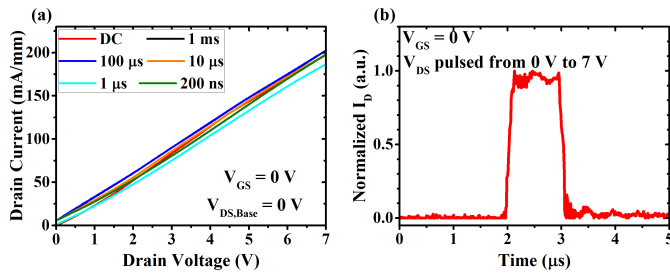


Fig. 6. (a) Drain turn on I_d - V_d curves for various pulse widths at $V_{gs} = 0$ showing negligible current dispersion compared to Fig. 8(b). (b) Drain turn on pulse with pulse width of $1 \mu s$ showing no trapping effects which reduces the plausibility of bulk traps causing the current dispersion.

conditions are used in this study and the fabrication flow does not involve high temperature ($> 520^\circ C$) processes. If both drain and gate are pulsed, we see change in the device characteristics as seen in Fig. 7. This is due to the gate lag effect caused by interface traps which is discussed in the next section.

Gate Turn On: Figure 8(a) shows DC and and gate pulsed I_d - V_d characteristics of the unpassivated device, we can clearly see severe DC-RF dispersion and knee-walk off. The current collapse during gate turn on pulse could be related to both traps directly under the gate electrode and the traps in the gate to drain access region [52]. Fig. 8(b) shows the I_d - V_d at a constant V_{gs} as a function of pulse width. The current collapse increases with decreasing pulse widths. As discussed in the previous section buffer traps are ruled out. The dispersion is caused by interface traps under the gate and in the gate-drain access region.

Fig.9 (a) shows the temperature dependent time domain plot of drain current response to a $1 ms$ gate turn on pulse. At all temperatures the drain current pulse shows a delayed asymptotic turn on transient which could be associated with emission time constants of electrons from the traps both in the gate-drain access region and the gate region. This pulse profile makes it self-explanatory as to why we see an increased current dispersion between static and pulsed I_d - V_d data with reduced pulse widths. A similar behaviour is seen during the turn off transient edge of I_d pulse which could be attributed to capture time constants of electrons by the interface traps. Increasing the temperature, marginally affects the capture and emission time constants thus accounting for

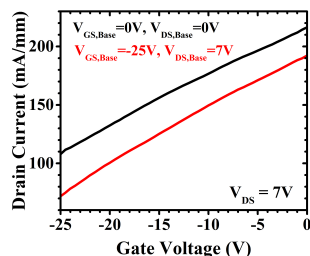


Fig. 7. Double pulsed transfer curves using a $50 \mu s$ pulse width for both gate and drain voltage pulses using the quiescent bias conditions as indicated in the figure. The black curve represents minimum trapping and hence more drain current levels while the red curve has reduced current due to trapping.

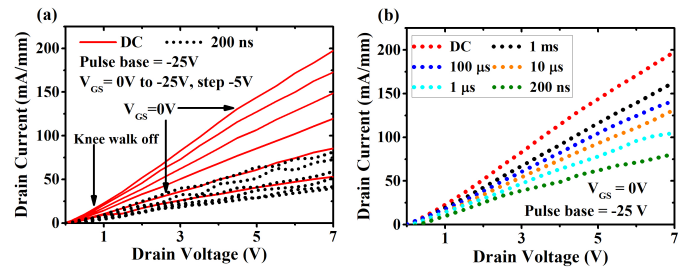


Fig. 8. (a) Drain current profiles for $V_g = 0V$ to $V_g = -25V$ for DC (red solid lines) and $200 ns$ pulse width (black dotted lines), before passivation. (b) Complete I_d - V_d profile from DC to $200 ns$ pulse width before passivation for $V_g = -0V$ shows clear dispersion in drain current with decreasing pulse width.

the slight difference in pulse shapes for different temperatures. Inset of Fig. 9(a) shows extended turn off transient for room temperature pulse to illustrate the slow capture process of electrons by traps after the gate voltage pulse returns to it's base value. As shown in Fig. 9(b), more negative the base voltage of the pulse, greater is the current collapse for the same pulse width. This is obvious since more negative base voltage would trigger more trapping of charges due to which drain current takes longer time to recover.

C. SiN_x passivation

According to the reports in previous studies on AlGaIn/GaN devices [51], [54]–[56], SiN_x passivation has helped create a near ideal semiconductor-dielectric interface by neutralizing the surface charge due to defects, dangling bonds and charged residuals. We explore the effect of SiN_x passivated on RIE treated Ga_2O_3 devices.

Fig. 10 compares pulsed I-V plots of the device post passivation with that of before passivation. We see a reduced DC-RF dispersion after passivation especially the low frequency dispersion is significantly reduced confirming that the role of traps in the gate-drain access region. While I_d - V_d data corresponding to $1 \mu s$ and $200 ns$ pulse widths still show dispersion, they both show considerable improvement in I_d value over unpassivated device. The most likely reason for this dispersion

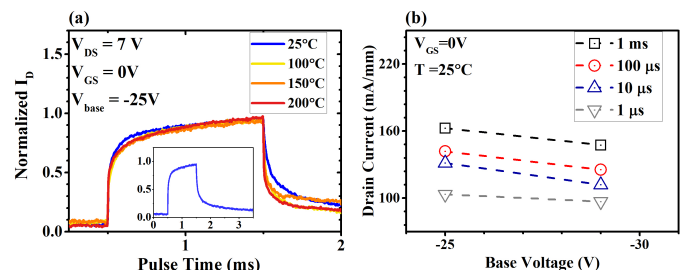


Fig. 9. (a) Temperature dependent drain current pulse profile for a $1 ms$ gate turn on pulse. Graph indicates how the traps response with temperature affects the drain current transient. Inset is room temperature plot for the same pulse width with extended turn off transient showing delayed effect due to capture time constants related to traps. (b) Change in maximum drain current recorded at $V_{gs} = 0V$ depending on the base voltage of the pulse for varying pulse widths as indicated. A more negative base voltage assists more trapping and thus more current collapse.

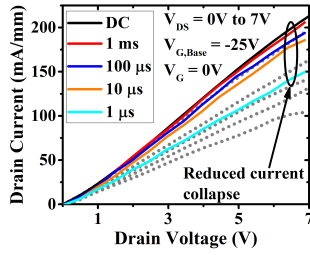


Fig. 10. Complete I_d - V_d profile from DC to 200 ns pulse width before (dotted grey lines) and after (solid lines) passivation for $V_g = -0V$ shows significant improvement in drain current dispersion down to 10 μs pulse width.

is traps under the gate which are still in play. The temperature dependent drain current transients in Fig. 11 clearly show the reduction of low frequency dispersion. Compared to the unpassivated drain current pulse, the passivated data is close to ideal square wave pulse shape except a very small delay at the end of the turn on and turn off transient which is responsible for the current dispersion seen in shorter pulse widths. High temperature pulse also shows a consistent improvement over its corresponding unpassivated pulse.

To get a more quantitative idea of the effect of passivation on current collapse we have calculated percentage current collapse in relation to DC data as a function of temperature and pulse width using following equations:

$$\Delta I_{cc,PW} = \frac{I_{d,DC} - I_{d,PW}}{I_{d,DC}} \quad (1)$$

$$\Delta I_{cc,temp} = \frac{I_{d,DC} - I_{d,1\mu s}}{I_{d,DC}} \quad (2)$$

where $I_{d,DC}$ is static drain current value during DC measurement, $I_{d,PW}$ is drain current measured for one of the five pulse widths, and $I_{d,1\mu s}$ is drain current measured for 1 μs pulse. All the drain current values are measured at $V_{ds} = 7V$ and $V_{gs} = 0V$. As can be seen in Fig. 12 (a) current collapse is almost entirely recovered for larger pulse widths down to 10 μs with collapse ratios below 10% whereas the smaller pulse widths (1 μs and 200 ns) still show more than 30% current collapse. The temperature dependent current collapse ratio for 1 μs pulse also shows average 20% improvement over unpassivated data. The monotonous increase in current collapse with temperature is most likely attributed to higher rate of trapping at elevated temperatures. It is clear that the

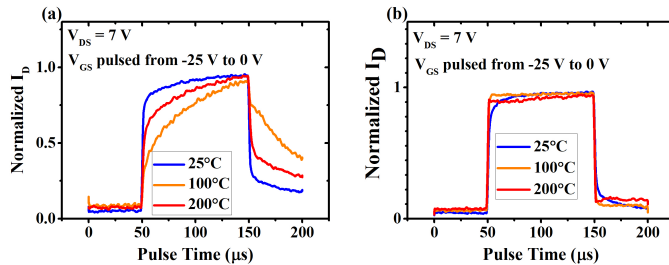


Fig. 11. Temperature dependent drain current pulse profile for a 100 μs gate turn on pulse before (a) and after (b) passivation.

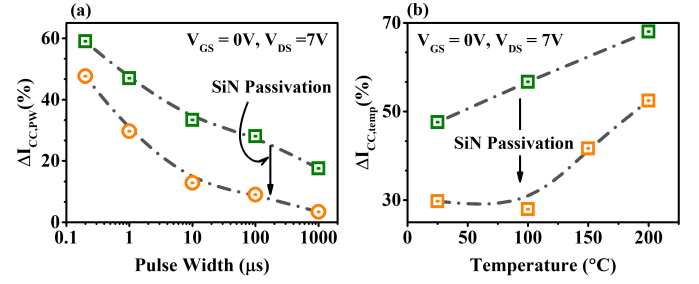


Fig. 12. (a) Percentage drain current collapse with respect to DC measurement as a function of pulse widths before (green squares) and after (orange circles) passivation. (b) Percentage drain current collapse with respect to DC measurement as a function of temperature before (green squares) and after (orange circles) passivation.

SiN_x is effective in passivation of low frequency traps in the drain access regions. Further optimization of the passivation can completely eliminate the high frequency dispersion.

D. Dynamics of traps

Following the data and analysis in previous subsections we discuss the origin of the DC-RF dispersion. Since it is highly unlikely that as grown MBE substrate had a high concentration of surface traps, reactive ion etching step is responsible for the defect related interface traps observed in this study. A comparison with other published results shows that similar DC-RF dispersion was seen in [44] which used RIE for the channel layer. There has been report of RIE induced channel depletion in Ga_2O_3 MESFETs [50]. While devices where the channel is not exposed to RIE [45], [46] show negligible DC-RF dispersion. Thus, the most likely cause of the dispersion in these devices are caused by RIE induced traps. During etching, Ga vacancies are created which leave behind three dangling O bonds that acts as a triple acceptor site according to McClusky *et al.* [57]. These traps form a virtual gate leading to depletion of electrons in drain access region which has slow turn on time when the gate is turned on.

The detrapping of electrons and hence the time response can occur by two possible methods: 1) thermionic emission from the trap, the rate for which is governed by the temperature of operation and/or 2) variable range hopping as described in [35].

Assuming a discrete or narrow band of traps in terms of energy level, the time constant of the traps can be determined by curve fitting a stretched exponential function in Eq. 3 to the drain current transient as shown in Fig. 13 (a).

$$I_{d,slow} = 1 - \exp\left(-\frac{t}{\tau}\right)^\beta \quad (3)$$

where $I_{d,slow}$ is the normalized slow transient, τ is the time constant and β is the fitting parameter. A slow time constant of 421 μs is obtained. From this time constant, the trap level is calculated [58] using Eq. 4 .

$$E_c - E_t = kT \cdot \ln\left(\frac{\tau \sigma_n \nu_n g_1 N_c}{g_0}\right) \quad (4)$$

where E_c, E_t are conduction band edge and trap energy levels respectively, σ_n is electron capture cross section of

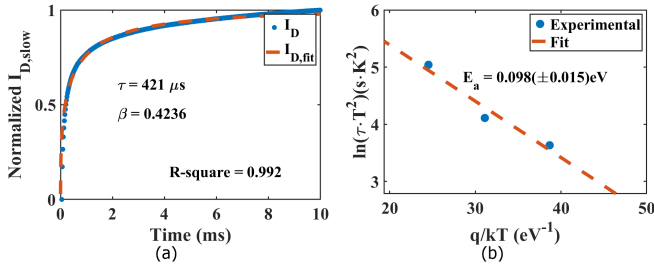


Fig. 13. (a) A normalized $I_{D,slow}$ and a stretched exponential fitted curve gives a fitting parameter $\beta = 0.4236$ and time constant $\tau = 421 \mu s$. (b) Arrhenius plot of q/kT vs $\ln(\tau \cdot T^2)$. Slope of linear fitting line gives activation energy for the trap.

the trap, ν_n is the thermal velocity of electron, g_0/g_1 is degeneracy of the trap when it is occupied by 0/1 electron and N_c is conduction band density of states. Assuming $\sigma_n = 10^{-15} \text{ cm}^2$, $\nu_n = 10^7 \text{ cm/s}$, $N_c = 3.72 \times 10^{18} \text{ cm}^{-3}$ for this calculation. The calculated trap level is deep with an energy level of 0.41 eV below conduction band. However, a deep trap such as 0.41 eV would present decreasing time constant with increasing temperature according to Shockley-Read-Hall recombination theory [59], which is not observed here (see Fig. 3 (b)).

An alternative mechanism suggested by Meneghesso *et al* [35] where the variable range hopping is the rate limiting step can explain the observed data. Following their approach, we use the Arrhenius equation fitting to q/kT vs $\ln(\tau T^2)$ plot, which gives a lower activation energy to be $0.098 \pm 0.015 \text{ eV}$ as shown in Fig. 13 (b). The trap level estimated from Fig. 13 (b) corresponds to a relatively shallow acceptor trap which along with a variable range hopping induced delay in capture and emission could be a more plausible explanation. Being a slow process VRH manifests itself as a slow turn on transient of the drain pulse with respect to time as seen in Fig. 9(a). Further experiments such as DLTS are necessary to confirm the location and physical origin of the traps.

E. High Frequency Characterization

High frequency performance of the device was measured to primarily compare the data before and after passivation and to highlight the effects of surface traps on cutoff frequency (f_t). The device performance was degraded by high source and drain resistances and lower current modulation due to thicker channel in addition to trap induced increase in access resistance which is evident from the very low f_t close to 100 MHz before passivation in Fig. 14 (blue circles). Passivation improves the cutoff frequency by approximately two times which is due to reduced trapping in the access region that improves the transient characteristics of the device but could still be limited by the high source drain resistances and trapping directly under the gate unaffected by passivation. Temperature dependent f_t measurement in Fig. 14 shows increase in cutoff frequency with temperature with a high f_t close to 1 GHz at 200°C (red spheres). This could be attributed to both slightly decreased source and drain contact resistance and possibly high temperature assisted faster emission of trapped electrons

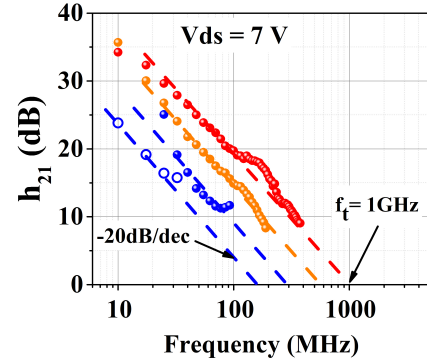


Fig. 14. h_{21} plots for various temperatures before passivation (hollow blue circles) and after passivation (spheres). Room temperature (blue spheres), 100°C (orange spheres) and 200°C (red spheres) indicate improvement in f_t with increasing temperature.

under the gate.

IV. CONCLUSION

We successfully fabricated a depletion mode Ga_2O_3 MOS-FET with a $0.12 \mu\text{m}$ gate length with a drain current of 210 mA/mm . Unpassivated devices show DC-RF dispersion with a peak current collapse ratio of 60% at for 200 ns gate turn on pulse. SiNx passivation show significant decrease in the current collapse. While the low frequency dispersion is eliminated the high frequency dispersion was present likely due to the traps under the gate. We also recorded a two fold improvement in cut-off frequency for room temperature measurements after passivation. A trap time constant of $421 \mu\text{s}$ was obtained from stretched exponential curve fitting to the drain current pulse from the room temperature pulsed current-voltage measurements.

We have shown that RIE damage is likely responsible for the Ga vacancies acting as acceptor like traps which induce a virtual gate in the access region between gate and drain which in turn is responsible for the current collapse observed in the transient response analysis of the device. The plasma damage also creates traps under the gate which modulate the threshold voltage of the device based on the temperature response of these traps. We also showed that the current dispersion can be mitigated, to some degree, by using a thick passivation layer of a silicon nitride. We investigated analytical response of the traps using stretched exponential curve fitting and provided a best fit explanation for the observed facts. Based on temperature dependent data, the variable range hopping based theory aligns much better with observed results than a pure Shockley-Read-Hall recombination theory.

REFERENCES

- [1] H. H. Tippins, "Optical absorption and photoconductivity in band edge of beta-ga2o3," *Physical Review*, vol. 140, no. 1a, pp. A316-&, 1965.
- [2] J. B. Varley, J. R. Weber, A. Janotti, and C. G. V. d. Walle, "Oxygen vacancies and donor impurities in β -ga2o3," *Applied Physics Letters*, vol. 97, no. 14, p. 142106, 2010.
- [3] K. Konishi, K. Goto, H. Murakami, Y. Kumagai, A. Kuramata, S. Yamakoshi, and M. Higashiwaki, "1-kv vertical ga2o3 field-plated schottky barrier diodes," *Applied Physics Letters*, vol. 110, no. 10, 2017.

- [4] M. Higashiwaki, K. Sasaki, A. Kuramata, T. Masui, and S. Yamakoshi, "Gallium oxide (β -Ga₂O₃) metal-semiconductor field-effect transistors on single-crystal β -Ga₂O₃ (010) substrates," *Applied Physics Letters*, vol. 100, no. 1, p. 013504, 2012.
- [5] S. Kohei, K. Akito, M. Takekazu, G. V. Encarnación, S. Kiyoshi, and Y. Shigenobu, "Device-quality β -Ga₂O₃ epitaxial films fabricated by ozone molecular beam epitaxy," *Applied Physics Express*, vol. 5, no. 3, p. 035502, 2012.
- [6] K. D. Chabak, N. Moser, A. J. Green, D. E. Walker, S. E. Tetlak, E. Heller, A. Crespo, R. Fitch, J. P. McCandless, K. Leedy, M. Baldini, G. Wagner, Z. Galazka, X. Li, and G. Jessen, "Enhancement-mode Ga₂O₃ wrap-gate fin field-effect transistors on native (100) β -Ga₂O₃ substrate with high breakdown voltage," *Applied Physics Letters*, vol. 109, 2016.
- [7] C. Joishi, S. Rafique, Z. Xia, L. Han, S. Krishnamoorthy, Y. Zhang, S. Lodha, H. Zhao, and S. Rajan, "Low-pressure cvd-grown β -Ga₂O₃ bevel-field-plated schottky barrier diodes," *Applied Physics Express*, vol. 11, no. 3, p. 031101, 2018.
- [8] A. A. U. Bhuiyan, Z. Feng, J. M. Johnson, H. L. Huang, J. Hwang, and H. Zhao, "Mocvd epitaxy of ultra-wide bandgap β -(Al_xGa_{1-x})₂O₃ with high-Al composition on (100) β -Ga₂O₃ substrates," *Crystal Growth & Design*, 2020.
- [9] A. Anhar Uddin Bhuiyan, Z. Feng, J. M. Johnson, Z. Chen, H.-L. Huang, J. Hwang, and H. Zhao, "Mocvd epitaxy of β -(Al_xGa_{1-x})₂O₃ thin films on (010) Ga₂O₃ substrates and n-type doping," *Applied Physics Letters*, vol. 115, no. 12, p. 120602, 2019.
- [10] K. Sasaki, A. Kuramata, T. Masui, E. G. Villora, K. Shimamura, and S. Yamakoshi, "Device-quality β -Ga₂O₃ epitaxial films fabricated by ozone molecular beam epitaxy," *Applied Physics Express*, vol. 5, no. 3, p. 035502, 2012.
- [11] H. Murakami, K. Nomura, K. Goto, K. Sasaki, K. Kawara, Q. T. Thieu, R. Togashi, Y. Kumagai, M. Higashiwaki, A. Kuramata, et al., "Homoepitaxial growth of β -Ga₂O₃ layers by halide vapor phase epitaxy," *Applied Physics Express*, vol. 8, no. 1, p. 015503, 2014.
- [12] K. Goto, K. Konishi, H. Murakami, Y. Kumagai, B. Monemar, M. Higashiwaki, A. Kuramata, and S. Yamakoshi, "Halide vapor phase epitaxy of Si doped β -Ga₂O₃ and its electrical properties," *Thin Solid Films*, vol. 666, pp. 182–184, 2018.
- [13] Y. Zhang, F. Alema, A. Mauze, O. S. Koksaldi, R. Miller, A. Osinsky, and J. S. Speck, "Mocvd grown epitaxial β -Ga₂O₃ thin film with an electron mobility of 176 cm²/V s at room temperature," *APL Materials*, vol. 7, no. 2, p. 022506, 2019.
- [14] S.-H. Han, A. Mauze, E. Ahmadi, T. Mates, Y. Oshima, and J. S. Speck, "n-type dopants in (001) β -Ga₂O₃ grown on (001) β -Ga₂O₃ substrates by plasma-assisted molecular beam epitaxy," *Semiconductor Science and Technology*, vol. 33, no. 4, p. 045001, 2018.
- [15] K. Zeng, A. Vaidya, and U. Singiseti, "1.85 kV breakdown voltage in lateral field-plated Ga₂O₃ mosfets," *IEEE Electron Device Letters*, vol. 39, no. 9, pp. 1385–1388, 2018.
- [16] K. Zeng, A. Vaidya, and U. Singiseti, "A field-plated Ga₂O₃ mosfet with near 2-kV breakdown voltage and 520 mW/cm² on-resistance," *Applied Physics Express*, vol. 12, no. 8, p. 081003, 2019.
- [17] Z. Hu, H. Zhou, K. Dang, Y. Cai, Z. Feng, Y. Gao, Q. Feng, J. Zhang, and Y. Hao, "Lateral β -Ga₂O₃ schottky barrier diode on sapphire substrate with reverse blocking voltage of 1.7 kV," *IEEE Journal of the Electron Devices Society*, vol. 6, pp. 815–820, 2018.
- [18] Z. Hu, K. Nomoto, W. Li, Z. Zhang, N. Tanen, Q. T. Thieu, K. Sasaki, A. Kuramata, T. Nakamura, D. Jena, et al., "Breakdown mechanism in 1 kA/cm² and 960 V e-mode β -Ga₂O₃ vertical transistors," *Applied Physics Letters*, vol. 113, no. 12, p. 122103, 2018.
- [19] Z. Hu, K. Nomoto, W. Li, N. Tanen, K. Sasaki, A. Kuramata, T. Nakamura, D. Jena, and H. G. Xing, "Enhancement-mode Ga₂O₃ vertical transistors with breakdown voltage \geq 1 kV," *IEEE Electron Device Letters*, vol. 39, no. 6, pp. 869–872, 2018.
- [20] W. Li, Z. Hu, K. Nomoto, Z. Zhang, J.-Y. Hsu, Q. T. Thieu, K. Sasaki, A. Kuramata, D. Jena, and H. G. Xing, "1230 V β -Ga₂O₃ trench schottky barrier diodes with an ultra-low leakage current of 1μ A/cm²," *Applied Physics Letters*, vol. 113, no. 20, p. 202101, 2018.
- [21] K. Tetzner, E. B. Treidel, O. Hilt, A. Popp, S. B. Anooz, G. Wagner, A. Thies, K. Ickert, H. Gargouri, and J. Würfl, "Lateral 1.8 kV β -Ga₂O₃ mosfet with 155 mW/cm² power figure of merit," *IEEE Electron Device Letters*, vol. 40, no. 9, pp. 1503–1506, 2019.
- [22] S. Sharma, K. Zeng, S. Saha, and U. Singiseti, "Field-plated lateral Ga₂O₃ mosfets with polymer passivation and 8.03 kV breakdown voltage," *IEEE Electron Device Letters*, vol. 41, no. 6, pp. 836–839, 2020.
- [23] Z. Hu, H. Zhou, Q. Feng, J. Zhang, C. Zhang, K. Dang, Y. Cai, Z. Feng, Y. Gao, X. Kang, et al., "Field-plated lateral β -Ga₂O₃ schottky barrier diode with high reverse blocking voltage of more than 3 kV and high dc power figure-of-merit of 500 mW/cm²," *IEEE Electron Device Letters*, vol. 39, no. 10, pp. 1564–1567, 2018.
- [24] J. K. Mun, K. Cho, W. Chang, H.-W. Jung, and J. Do, "2.32 kV breakdown voltage lateral β -Ga₂O₃ mosfets with source-connected field plate," *ECS Journal of Solid State Science and Technology*, vol. 8, no. 7, p. Q3079, 2019.
- [25] K. Konishi, K. Goto, H. Murakami, Y. Kumagai, A. Kuramata, S. Yamakoshi, and M. Higashiwaki, "1-kV vertical Ga₂O₃ field-plated schottky barrier diodes," *Applied Physics Letters*, vol. 110, no. 10, p. 103506, 2017.
- [26] H. Gong, X. Chen, Y. Xu, F.-F. Ren, S. Gu, and J. Ye, "A 1.86-kV double-layered NiO/ β -Ga₂O₃ vertical p-n heterojunction diode," *Applied Physics Letters*, vol. 117, no. 2, p. 022104, 2020.
- [27] X. Huang, F. Liao, L. Li, X. Liang, Q. Liu, C. Zhang, and X. Hu, "3.4 kV breakdown voltage Ga₂O₃ trench schottky diode with optimized trench corner radius," *ECS Journal of Solid State Science and Technology*, vol. 9, no. 4, p. 045012, 2020.
- [28] K. Ghosh and U. Singiseti, "Ab initio velocity-field curves in monoclinic β -Ga₂O₃," *Journal of Applied Physics*, vol. 122, no. 3, p. 035702, 2017.
- [29] Y. Zhang, Z. Xia, J. Mcglone, W. Sun, C. Joishi, A. R. Arehart, S. A. Ringel, and S. Rajan, "Evaluation of low-temperature saturation velocity in β -(Al_xGa_{1-x})₂O₃/Ga₂O₃ modulation-doped field-effect transistors," *IEEE Transactions on Electron Devices*, vol. 66, no. 3, pp. 1574–1578, 2019.
- [30] A. J. Green, K. D. Chabak, M. Baldini, N. Moser, R. C. Gilbert, R. Fitch, G. Wagner, Z. Galazka, J. McCandless, and A. Crespo, " β -Ga₂O₃ mosfets for radio frequency operation," *IEEE Electron Device Letters*, 2017.
- [31] K. D. Chabak, D. E. Walker, A. J. Green, A. Crespo, M. Lindquist, K. Leedy, S. Tetlak, R. Gilbert, N. A. Moser, and G. Jessen, "Submicron gallium oxide radio frequency field-effect transistors," in *2018 IEEE MTT-S International Microwave Workshop Series on Advanced Materials and Processes for RF and THz Applications (IMWS-AMP)*, pp. 1–3.
- [32] M. H. Takafumi Kamimura, Y. N., "Rf small-signal characteristics and delay time analysis of submicron Ga₂O₃ mosfets," in *The 78th Device Research Conference*, IEEE.
- [33] Z. Xia, H. Xue, C. Joishi, J. Mcglone, N. K. Kalarickal, S. H. Sohel, M. Brenner, A. Arehart, S. Ringel, S. Lodha, W. Lu, and S. Rajan, " β -Ga₂O₃ delta-doped field-effect transistors with current gain cutoff frequency of 27 GHz," *IEEE Electron Device Letters*, vol. 40, no. 7, pp. 1052–1055, 2019.
- [34] M. Faqir, G. Verzellesi, A. Chini, F. Fantini, F. Danesin, G. Meneghesso, E. Zanoni, and C. Dua, "Mechanisms of rf current collapse in AlGaN-GaN high electron mobility transistors," *IEEE Transactions on Device and Materials Reliability*, vol. 8, no. 2, pp. 240–247, 2008.
- [35] G. Meneghesso, M. Meneghini, D. Bisi, I. Rossetto, A. Cester, U. K. Mishra, and E. Zanoni, "Trapping phenomena in AlGaN/GaN HEMTs: a study based on pulsed and transient measurements," *Semiconductor Science and Technology*, vol. 28, no. 7, p. 074021, 2013.
- [36] J. M. Tirado, J. L. Sanchez-Rojas, and J. I. Izpura, "Trapping effects in the transient response of AlGaN/GaN HEMT devices," *IEEE Transactions on Electron Devices*, vol. 54, no. 3, pp. 410–417, 2007.
- [37] G. Meneghesso, G. Verzellesi, R. Pierobon, F. Rampazzo, A. Chini, U. K. Mishra, C. Canali, and E. Zanoni, "Surface-related drain current dispersion effects in AlGaN-GaN HEMTs," *IEEE Transactions on Electron Devices*, vol. 51, no. 10, pp. 1554–1561, 2004.
- [38] R. Vetury, N. Q. Zhang, S. Keller, and U. K. Mishra, "The impact of surface states on the dc and rf characteristics of AlGaN/GaN HEMTs," *IEEE Transactions on Electron Devices*, vol. 48, no. 3, pp. 560–566, 2001.
- [39] G. Verzellesi, R. Pierobon, F. Rampazzo, G. Meneghesso, A. Chini, U. K. Mishra, C. Canali, and E. Zanoni, "Experimental/numerical investigation on current collapse in AlGaN/GaN HEMTs," in *Digest. International Electron Devices Meeting*, pp. 689–692.
- [40] Z. Yatabe, J. T. Asubar, T. Sato, and T. Hashizume, "Interface trap states in Al₂O₃/AlGaN/GaN structure induced by inductively coupled plasma etching of AlGaN surfaces," *physica status solidi (a)*, vol. 212, no. 5, pp. 1075–1080, 2015.
- [41] M. Mamor and A. Sellai, "Characterization of plasma etching induced interface states at Ti-p-SiGe schottky contacts," *Journal of Vacuum Science & Technology A*, vol. 26, no. 4, pp. 705–709, 2008.
- [42] K.-C. Huang, W.-H. Lan, and K. F. Huang, "Inductively coupled plasma reactive ion etching-induced GaN defect studied by schottky current transport analysis," *Japanese Journal of Applied Physics*, vol. 43, no. 1, pp. 82–85, 2004.
- [43] S. Kim, Y. Hori, W.-C. Ma, D. Kikuta, T. Narita, H. Iguchi, T. Uesugi, T. Kachi, and T. Hashizume, "Interface properties of Al₂O₃/n-GaN struc-

- tures with inductively coupled plasma etching of gan surfaces,” *Japanese Journal of Applied Physics*, vol. 51, p. 0201, 2012.
- [44] N. A. Moser, T. Asel, K. J. Liddy, M. Lindquist, N. C. Miller, S. Mou, A. Neal, D. E. Walker, S. Tetlak, K. D. Leedy, G. H. Jessen, A. J. Green, and K. D. Chabak, “Pulsed power performance of β -ga2o3 mosfets at l-band,” *IEEE Electron Device Letters*, vol. 41, no. 7, pp. 989–992, 2020.
- [45] N. A. Moser, J. P. McCandless, A. Crespo, K. D. Leedy, A. J. Green, E. R. Heller, K. D. Chabak, N. Peixoto, and G. H. Jessen, “High pulsed current density β -ga2o3 mosfets verified by an analytical model corrected for interface charge,” *Applied Physics Letters*, vol. 110, no. 14, p. 143505, 2017.
- [46] M. Singh, M. A. Casbon, M. J. Uren, J. W. Pomeroy, S. Dalcanale, S. Karboyan, P. J. Tasker, M. H. Wong, K. Sasaki, A. Kuramata, S. Yamakoshi, M. Higashiwaki, and M. Kuball, “Pulsed large signal rf performance of field-plated ga2o3 mosfets,” *IEEE Electron Device Letters*, vol. 39, no. 10, pp. 1572–1575, 2018.
- [47] J. F. McGlone, Z. Xia, C. Joishi, S. Lodha, S. Rajan, S. Ringel, and A. R. Arehart, “Identification of critical buffer traps in si δ -doped β -ga2o3 mesfets,” *Applied Physics Letters*, vol. 115, no. 15, p. 153501, 2019.
- [48] C. Joishi, Z. Xia, J. McGlone, Y. Zhang, A. R. Arehart, S. Ringel, S. Lodha, and S. Rajan, “Effect of buffer iron doping on delta-doped β -ga2o3 metal semiconductor field effect transistors,” *Applied Physics Letters*, vol. 113, no. 12, p. 123501, 2018.
- [49] J. F. McGlone, Z. Xia, Y. Zhang, C. Joishi, S. Lodha, S. Rajan, S. A. Ringel, and A. R. Arehart, “Trapping effects in si δ -doped β -ga2o3 mesfets on an fe-doped β -ga2o3 substrate,” *IEEE Electron Device Letters*, vol. 39, no. 7, pp. 1042–1045, 2018.
- [50] C. Joishi, Z. Xia, J. S. Jamison, S. H. Sohler, R. C. Myers, S. Lodha, and S. Rajan, “Deep-recessed β -ga2o3 delta-doped field-effect transistors with in situ epitaxial passivation,” *IEEE Transactions on Electron Devices*, vol. 67, no. 11, pp. 4813–4819, 2020.
- [51] S. C. Binari, P. B. Klein, and T. E. Kazior, “Trapping effects in wide-bandgap microwave fets,” in *2002 IEEE MTT-S International Microwave Symposium Digest (Cat. No.02CH37278)*, vol. 3, pp. 1823–1826 vol.3, 2002.
- [52] S. C. Binari, P. Klein, and T. E. Kazior, “Trapping effects in gan and sic microwave fets,” *Proceedings of the IEEE*, vol. 90, no. 6, pp. 1048–1058, 2002.
- [53] M. H. Wong, K. Sasaki, A. Kuramata, S. Yamakoshi, and M. Higashiwaki, “Anomalous fe diffusion in si-ion-implanted β -ga2o3 and its suppression in ga2o3 transistor structures through highly resistive buffer layers,” *Applied Physics Letters*, vol. 106, no. 3, p. 032105, 2015.
- [54] T. Hashizume, S. Ootomo, T. Inagaki, and H. Hasegawa, “Surface passivation of gan and gan/algan heterostructures by dielectric films and its application to insulated-gate heterostructure transistors,” *Journal of Vacuum Science & Technology B: Microelectronics and Nanometer Structures Processing, Measurement, and Phenomena*, vol. 21, no. 4, pp. 1828–1838, 2003.
- [55] K. Hyungtak, R. M. Thompson, V. Tilak, T. R. Prunty, J. R. Shealy, and L. F. Eastman, “Effects of sin passivation and high-electric field on algan-gan hfet degradation,” *IEEE Electron Device Letters*, vol. 24, no. 7, pp. 421–423, 2003.
- [56] B. M. Green, K. K. Chu, E. M. Chumbes, J. A. Smart, J. R. Shealy, and L. F. Eastman, “The effect of surface passivation on the microwave characteristics of undoped algan/gan hemts,” *IEEE Electron Device Letters*, vol. 21, no. 6, pp. 268–270, 2000.
- [57] M. D. McCluskey, “Point defects in ga2o3,” *Journal of Applied Physics*, vol. 127, no. 10, p. 101101, 2020.
- [58] R. Coffie, *Characterizing and suppressing DC-to-RF dispersion in AlGaNGaN high electron mobility transistors*. Phd thesis, 2003.
- [59] W. Shockley and W. T. Read, “Statistics of the recombinations of holes and electrons,” *Phys. Rev.*, vol. 87, pp. 835–842, Sep 1952.